Mechanics Research Communications 103 (2020) 103480

Contents lists available at ScienceDirect

Mechanics Research Communications

journal homepage: www.elsevier.com/locate/mechrescom

Design and control of tensegrity morphing airfoils

Muhao Chen[a,*], Jiacheng Liu[b], Robert E. Skelton[a]

[a] Department of Aerospace Engineering, Texas A&M University, College Station, TX, USA
[b] Department of Ocean Engineering, Texas A&M University, College Station, TX, USA

ARTICLE INFO

Article history:
Received 31 August 2019
Revised 13 January 2020
Accepted 14 January 2020
Available online 21 January 2020

Keywords:
Tensegrity structures
Morphing airfoil
Nonlinear dynamics
Nonlinear control
Integrating structure and control design

ABSTRACT

We present a general approach of design, dynamics, and control for tensegrity morphing airfoils. Firstly, based on reduced order Class-*k* tensegrity dynamics, a shape control law for tensegrity systems is derived. Then, we develop a method for discretizing continuous airfoil curves based on shape accuracy. This method is compared with conventional methods (i.e. evenly spacing and cosine spacing methods). A tensegrity topology for shape controllable airfoil is proposed. A morphing tensegrity airfoil example is given to demonstrate successful shape control. This work paves a road towards integrating structure and control design, the principles developed here can also be used for 3D morphing airfoil design and control of various kinds of tensegrity structures.

Published by Elsevier Ltd.

1. Introduction

The Wright Brothers made the first sustainable, controllable, powered, heavier than air manned flight in 1903. The fundamental breakthrough was their invention of a three-axis control method for improving fly control stability of the wing box structure by morphing the shape of the wing during flight [1].

Morphing airfoil is gaining significant attention by researchers with the thriving prosperity of the aerospace industry. Compared to a fixed-wing, a flexible profile is more adjustable to various flight conditions. The fundamental concept of achieving certain aerodynamic performance by means of changing the shape of a wing motivates us to solve the following problems: find an efficient airfoil structure and control laws to adjust various flight regimes. The existing morphing technologies (wing slats, flaps, spoiler, aileron, winglet, and trims) can achieve some desired performance. And many researchers have pointed out the challenges of this area. Sofla et al. [2], Lachenal et al. [3], Kuribayashi et al. [4], and Liu et al. [5] summarized shape morphing status and challenges, mainly focusing on the direction of shape memory alloys (SMA), piezoelectric actuators (PZT), shape memory polymers (SMP), and stimulus-responsive polymers (SRP). Valasek [6], Barbarino et al. [7], and Reich and Sanders [8] addressed important issues on morphing aircraft, bio-inspiration, smart structures, power requirements and smart actuators. Santer showed load-path-based topology optimization for adaptive wing structures [9,10]. However, few of them start with a system point of view to solve the structure and control problem in an integrative manner. This study presents our system which integrates structure and control designs using a novel tensegrity morphing airfoil.

Tensegrity is a network of bars and strings, where bars only take compression and strings only take tension [11]. Perhaps biological systems provide the greatest evidence that tensegrity concepts yield the most efficient structures [11], for example, the micromechanism of the spider fibers shows that the network structure has both tensile and compressive members [12]. There are many advantages of tensegrity: 1. All structural members are axially loaded, there is no material bending. 2. All the structure members are uni-directionally loaded, so there is no reversal of load direction, and the uncertainties of the 1-dimensional material movement bring better stability margins. 3. The structural efficiency in strength to mass is very high. 4. The tensegrity system is easy to integrate structure and control because the dynamic models are more accurate. A structural member can also serve as a sensor and actuator. The actuator and sensor architecture can be easily optimized. One can change shape/stiffness without changing stiffness/shape, and one can achieve minimal control energy (morphing from one equilibrium to another). The bar-string connection patterns are like 3D fibers that allow engineers and artists to knit any structure that physics and their imagination allow. This new dimension of engineering thought motivates engineers to rethink and study structures in a more fundamental way, for example, beam structures made of V-Expander cells [13,14], the mechanical response of 3D tensegrity lattices [15], high performance robotics

* Corresponding author.
E-mail addresses: muhaochen@tamu.edu (M. Chen), jiachengliu@tamu.edu (J. Liu), bobskelton@tamu.edu (R.E. Skelton).

https://doi.org/10.1016/j.mechrescom.2020.103480
0093-6413/Published by Elsevier Ltd.

[16–18], minimum mass bridge [19], deployable antenna [20], landers [21–24], tunable energy dissipation structure [25], and tensegrity spine [26,27], etc.

The conceptual design and physical model of the tensegrity wing are presented in the book Tensegrity System by Skelton and Mauricio 2009, which was a DARPA sponsored "smart structures" research program. The design in their book is a light weight fixed wing, composed of 2D airfoil solid pieces connected with tensegrity T-Bar topology [11]. Henrickson et al. [28] presents a 2D cross-bar topology airfoil (a class-1 tensegrity structure) design and demonstrate the morphing ability. These design shows the tensegrity system brings more functionalities to wing design such as minimum mass, deployability, and shape control. In a similar way to a bird's wing, the strings in the tensegrity wing are functioning as muscles to warp the whole wing to achieve various aerodynamic performance requirements. Some researchers have discussed their ideas in morphing wing design, for example, Moored studies the deflection [29] and shape optimization [30] of the wing in span-wise direction by tensegrity beams and plates, Jones shows his idea in fuzzy control strategy for morphing [31]. James presented a control theory to formulate computationally feasible procedures for aerodynamic design [32]. However, we argue that control design after wing design destroys the flying efficiency that is so carefully treated in the structure design in the first place [11]. Instead of using control systems to push the structure away from its equilibrium, we propose to simply modify the equilibrium of tensegrity structures to achieve the new desired shape with little control effort. As feedback, less control power also exerts less stress on structural components to accomplish the same objectives. Thus, the best performance cannot be achieved by separating structure and control designs. This paper starts from airfoil shape discretization methods, presents a practical airfoil topology design, and a nonlinear control law for any Class-k structures.

This paper is structured as follows: Section 2 introduces tensegrity principles, nonlinear Class-k dynamics, reduced-order form, and nonlinear shape control laws. Section 3 discusses the error bound method for continuous airfoil shape discretization and the design of tensegrity airfoils. Section 4 gives a case study and results. Section 5 presents the conclusions.

2. Tensegrity dynamics and control

2.1. Class-k tensegrity dynamics

The accurate quantitative knowledge of structural behavior should be given in a simple, compact form. Tensegrity dynamics were first analytically studied by Motro et al. in 1987 [33], since then many kinds of research followed. Skelton et al. introduced a non-minimal coordinates method without using the conventional angular velocities for rigid bodies [34] simplified the math a lot. Recent work by Goyal et al. give a complete description of tensegrity dynamics by including string mass, class-k bar-length correction, and analytic solutions of Lagrange multiplier Ω [35]:

$$\ddot{N}M_s + NK_s = W + \Omega P^T, \tag{1}$$

$$M_s = \left[C_{nb}^T\left(C_b^T\hat{J}C_b + C_r^T\hat{m}_bC_r\right)\ C_{ns}^T\hat{m}_s\right], \tag{2}$$

$$K_s = \left[C_s^T\hat{\gamma}C_{sb} - C_{nb}^TC_b^T\hat{\lambda}C_b\ C_s^T\hat{\gamma}C_{ss}\right], \tag{3}$$

where $\hat{\lambda}$ is:

$$\hat{\lambda} = -\hat{J}\hat{l}^{-2}\lfloor\dot{B}^T\dot{B}\rfloor - \frac{1}{2}\hat{l}^{-2}\lfloor B^T(W + \Omega P^T - S\hat{\gamma}C_s)C_{nb}^TC_b^T\rfloor, \tag{4}$$

and the operator $\lfloor\bullet\rfloor$ sets every off-diagonal element of the square matrix operand to zero, $N \in R^{3\times n}$ (n is the total number of nodes) is the nodal matrix with each column denotes x, y, and z coordinates of each node, $M_s \in R^{n\times n}$ is mass matrix of all the bars and strings, $K_s \in R^{n\times n}$ is the stiffness matrix, $W \in R^{3\times n}$ contains the external force at each node, $\Omega \in R^{3\times c}$ (c is number of constraints $NP = D$), the Lagrange multipliers required to maintain these constraints can be thought of as contact forces at the Class-k nodes [36]. Ω is the matrix of Lagrange multipliers associated with the constraint $NP = D$, $P \in R^{c\times n}$ is the constraint matrix, denoting which nodes are the Class-k nodes and which nodes are grounded. $B = \begin{bmatrix}\mathbf{b}_1 & \mathbf{b}_2 & \cdots & \mathbf{b}_\beta\end{bmatrix} \in R^{3\times\beta}$ and $S = \begin{bmatrix}\mathbf{s}_1 & \mathbf{s}_2 & \cdots & \mathbf{s}_\alpha\end{bmatrix} \in R^{3\times\sigma}$ ($\mathbf{b}_i$ and $\mathbf{s}_i$ are bar and string vectors, β and σ represent the number of bars and number of string) are bar and string matrices whose columns are bar or string vectors, C_b and C_s are the connectivity matrix of bars and strings (consists of a "−1" at the ith column, a "+1" at the jth column, and zeros elsewhere to define a structure member connecting from $\mathbf{n}_i$ to $\mathbf{n}_j$.), they satisfy $B = NC_b^T$ and $S = NC_s^T$. The nodes have two types: bar nodes $N_b \in R^{3\times 2\beta}$, which are the endpoints of bars, and string nodes $N_s \in R^{3\times\sigma}$, which are the locations of string-to-string connections that have a point mass associated with them, $N = \begin{bmatrix}N_b & N_s\end{bmatrix}$. Then, the bar and string nodes can be extracted from the node matrix N with the definition of two connectivity matrices, C_{nb} and C_{ns}. C_s is divided into two parts: the first, C_{sb}, describing bar-to-string joints and the second, C_{ss}, describing string-to-string joints. $\hat{\bullet}$ is an operator that converts a vector into a diagonal matrix. $\hat{m}_b$, $\hat{m}_s$, $\hat{\gamma}$, $\hat{\lambda}$ are bar mass, string mass, string force density, and bar force density matrices respectively. $\hat{J}$ is the bar moment of inertia matrix, which satisfies $J_i = \frac{m_{bi}}{12} + \frac{m_{bi}r_{bi}^2}{4l_i^2}$, and r_{bi} and l_i are the radius and length of the ith bar.

Adding the linear constraints to the dynamics will restrict the motion in certain dimensions. We separate the moving and stationary nodes by performing a Singular Value Decomposition of the matrix P to eliminate unnecessary computations of stationary nodes, the order of dynamics equation can be reduced into [35]:

$$\ddot{\eta}_2M_2 + \eta_2K_2 = \widetilde{W}, \tag{5}$$

where $\eta = [\eta_1\ \eta_2] \triangleq NU = [NU_1\ NU_2]$, $M_2 = U_2^TM_sU_2$, $K_2 = U_2^TK_sU_2$, $\widetilde{W} = WU_2 - \eta_1U_1^TK_sU_2$, $\eta_1 = DV\Sigma_1^{-1}$, $NP = D$, $P = U\Sigma V^T = \begin{bmatrix}U_1 & U_2\end{bmatrix}\begin{bmatrix}\Sigma_1\\0\end{bmatrix}V^T$.

2.2. Coordinate transformation

2.2.1. X matrix definition

From the above, the reduced order dynamics can be written in a standard second order differential equation form. Let X matrix be the product of the η_2 and M_2 matrices. Since M_2 is the mass matrix for the tensegrity system and it is non-singular, an expression for η_2 in terms of X can then be written as:

$$X = \eta_2M_2 \rightarrow \eta_2 = XM_2^{-1} \tag{6}$$

$$\dot{X} = \dot{\eta}_2M_2 \rightarrow \dot{\eta}_2 = \dot{X}M_2^{-1} \tag{7}$$

$$\ddot{X} = \ddot{\eta}_2M_2 \rightarrow \ddot{\eta}_2 = \ddot{X}M_2^{-1}. \tag{8}$$

2.2.2. Conversion of matrix dynamics

Substitute Eqs. (6)–(8) into Eq. (1), one can get:

$$\ddot{X} + XM_2^{-1}K_2 = \widetilde{W}. \tag{9}$$

Take the ith element of the first and second terms of the Eq. (4) and use the fact $\hat{\mathbf{x}}\mathbf{y} = \hat{\mathbf{y}}\mathbf{x}$, where $\mathbf{x}$ and $\mathbf{y}$ are vectors, Eq. (4) can be written as:

$$-\lambda_i = \frac{J_i||\dot{\mathbf{b}}_i||^2}{l_i^2} + \frac{1}{2l_i^2}\mathbf{b}_i^TWC_{nb}^TC_b^T\mathbf{e}_i + \frac{1}{2l_i^2}\mathbf{b}_i^T\Omega P^TC_{nb}^TC_b^T\mathbf{e}_i - \frac{1}{2l_i^2}\mathbf{b}_i^TSC_s\widehat{C_{nb}^TC_b^T}\mathbf{e}_i\gamma, \tag{10}$$

where $\mathbf{b_i}$ is the vector of each bar, $\mathbf{e}_i$ is a vector with 1 in the ith elements and zeros else where. Stack all the elements of vector λ we get:

$$-\lambda = \underbrace{\begin{bmatrix} \frac{J_1\|\dot{\mathbf{b}}_1\|^2}{l_1^2} + \frac{1}{2l_1^2}\mathbf{b}_1^T W C_{nb}^T C_b^T \mathbf{e}_1 + \frac{1}{2l_1^2}\mathbf{b}_1^T \Omega P^T C_{nb}^T C_b^T \mathbf{e}_1 \\ \vdots \\ \frac{J_i \| \dot{\mathbf{b}}_i\|^2}{l_i^2} + \frac{1}{2l_i^2}\mathbf{b}_i^T W C_{nb}^T C_b^T \mathbf{e}_i + \frac{1}{2l_i^2}\mathbf{b}_i^T \Omega P^T C_{nb}^T C_b^T \mathbf{e}_i \\ \vdots \\ \frac{J_\beta \| \dot{\mathbf{b}}_\beta\|^2}{l_\beta^2} + \frac{1}{2l_\beta^2}\mathbf{b}_\beta^T W C_{nb}^T C_b^T \mathbf{e}_\beta + \frac{1}{2l_\beta^2}\mathbf{b}_\beta^T \Omega P^T C_{nb}^T C_b^T \mathbf{e}_\beta \end{bmatrix}}_{\tau} - \underbrace{\begin{bmatrix} \frac{1}{2l_1^2}\mathbf{b}_1^T S C_s \widehat{C_{nb}^T C_b^T \mathbf{e}_1} \\ \vdots \\ \frac{1}{2l_i^2}\mathbf{b}_i^T S C_s \widehat{C_{nb}^T C_b^T \mathbf{e}_i} \\ \vdots \\ \frac{1}{2l_\beta^2}\mathbf{b}_\beta^T S C_s \widehat{C_{nb}^T C_b^T \mathbf{e}_\beta} \end{bmatrix}}_{\Lambda} \gamma. \tag{11}$$

We can express in a compact matrix form,

$$-\lambda = \Lambda\gamma + \tau. \tag{12}$$

2.3. Shape control law

2.3.1. Shape objectives

L specifies the axes of interest for the system nodes, R denotes which of those system nodes are nodes of interest. By multiplying $Y_c = L\eta_2 R$, one can, therefore, extract the current values of the node coordinates of interest for the node configuration N:

$$Y_c = LNU_2R = L\eta_2 R = LXM_2^{-1}R. \tag{13}$$

$\bar{Y}$ is a matrix containing the desired values for the node coordinates of interest. The error matrix E between the current and desired node coordinates of interest can then be written:

$$E = Y_c - \bar{Y}. \tag{14}$$

2.3.2. Error dynamics

To achieve the desired shape control, the error matrix E and its first and second-time derivatives should all go to zero. This goal is expressed as follows. Let Ψ and Φ be chosen matrices such that:

$$\ddot{E} + \Psi\dot{E} + \Phi E = 0 \tag{15}$$

is a stable equation about the value $E = 0$. Using Eqs. (9), (13), and (14), the Eq. (15) becomes:

$$L(\widetilde{W} - XM_2^{-1}K_2)M_2^{-1}R + \Psi L\dot{X}M_2^{-1}R + \Phi LXM_2^{-1}R - \Phi\bar{Y} = 0. \tag{16}$$

This can be expanded and rearranged:

$$LXM_2^{-1}K_2M_2^{-1}R = L\widetilde{W}M_2^{-1}R + \Psi L\dot{X}M_2^{-1}R + \Phi LXM_2^{-1}R - \Phi\bar{Y} \tag{17}$$

Substitute $K_2 = U_2^T K_s U_2$ and K_s from Eq. (3) into the left hand side of this equation:

$$\begin{aligned} LXM_2^{-1}K_2M_2^{-1}R &= LXM_2^{-1}U_2^T K_s U_2 M_2^{-1}R \\ &= LXM_2^{-1}U_2^T\begin{bmatrix} C_s^T\hat{\gamma}C_{sb} - C_{nb}^T C_b^T\hat{\lambda}C_b & C_s^T\hat{\gamma}C_{ss}\end{bmatrix}U_2M_2^{-1}R. \end{aligned} \tag{18}$$

Let us take a look at the mass matrix again,

$$M_2 = U_2^T M_s U_2$$

$$\begin{aligned} M_s &= \begin{bmatrix} C_{nb}^T\left(C_b^T\hat{J}C_b + C_r^T\hat{m}_b C_r\right) & C_{ns}^T\hat{m}_s\end{bmatrix} \\ &= \begin{bmatrix} C_b^T & C_r^T & 0 \\ 0 & 0 & I\end{bmatrix}\begin{bmatrix}\hat{J} & 0 & 0 \\ 0 & \hat{m}_b & 0 \\ 0 & 0 & \hat{m}_s\end{bmatrix}\begin{bmatrix} C_b & 0 \\ C_r & 0 \\ 0 & I\end{bmatrix} \end{aligned} \tag{19}$$

Using $\begin{bmatrix}\frac{1}{2}C_b^T & 2C_r^T\end{bmatrix}^{-1} = \begin{bmatrix} C_b^T & C_r^T\end{bmatrix}^T$, it can also be shown that:

$$\begin{bmatrix}\frac{1}{2}C_b^T & 2C_r^T & 0 \\ 0 & 0 & I\end{bmatrix}^{-1} = \begin{bmatrix} C_b & 0 \\ C_r & 0 \\ 0 & I\end{bmatrix}. \tag{20}$$

Then, M_s^{-1} can be obtained,

$$\begin{aligned} M_s^{-1} &= \begin{bmatrix}\frac{1}{2}C_b^T & 2C_r^T & 0 \\ 0 & 0 & I\end{bmatrix}\begin{bmatrix}\hat{J} & 0 & 0 \\ 0 & \hat{m}_b & 0 \\ 0 & 0 & \hat{m}_s\end{bmatrix}^{-1}\begin{bmatrix}\frac{1}{2}C_b & 0 \\ 2C_r & 0 \\ 0 & I\end{bmatrix} \\ &= \begin{bmatrix}\frac{1}{2}C_b^T & 2C_r^T & 0 \\ 0 & 0 & I\end{bmatrix}\begin{bmatrix}\hat{J} & 0 & 0 \\ 0 & \hat{m}_b & 0 \\ 0 & 0 & \hat{m}_s\end{bmatrix}^{-1}\begin{bmatrix}\frac{1}{2}C_bC_{nb} \\ 2C_rC_{nb} \\ C_{ns}\end{bmatrix} \\ &= \begin{bmatrix}\frac{1}{4}C_b^T\hat{J}^{-1}C_bC_{nb} + 4C_r^T\hat{m}_b^{-1}C_rC_{nb} \\ \hat{m}_s^{-1}C_{ns}\end{bmatrix}. \end{aligned} \tag{21}$$

Let $M_{s1} = \frac{1}{4}C_b^T\hat{J}^{-1}C_bC_{nb} + 4C_r^T\hat{m}_b^{-1}C_rC_{nb}$ and $M_{s2} = \hat{m}_s^{-1}C_{ns}$, M_s can be simply written as $M_s = \begin{bmatrix} M_{s1} \\ M_{s2}\end{bmatrix}$. Then, $M_2^{-1} = U_2^T\begin{bmatrix} M_{s1} \\ M_{s2}\end{bmatrix}U_2$.

Eq. (18) can be written as:

$$\begin{aligned} LXM_2^{-1}K_2M_2^{-1}R = LXM_2^{-1}U_2^T(&C_s^T\hat{\gamma}C_{sb}M_{s1} \\ &- C_{nb}^TC_b^T\hat{\lambda}C_bM_{s1} + C_s^T\hat{\gamma}C_{ss}M_{s2})U_2R. \end{aligned} \tag{22}$$

Take the ith column on both sides,

$$\begin{aligned} LXM_2^{-1}K_2M_2^{-1}R\mathbf{e}_i = LXM_2^{-1}U_2^T(&C_s^T\hat{\gamma}C_{sb}M_{s1}U_2R\mathbf{e}_i \\ &- C_{nb}^TC_b^T\hat{\lambda}C_bM_{s1}U_2R\mathbf{e}_i + C_s^T\hat{\gamma}C_{ss}M_{s2}U_2R\mathbf{e}_i). \end{aligned} \tag{23}$$

Using the fact $\hat{\mathbf{x}}\mathbf{y} = \hat{\mathbf{y}}\mathbf{x}$, we have:

$$\begin{aligned} LXM_2^{-1}K_2M_2^{-1}R\mathbf{e}_i = LXM_2^{-1}U_2^T(&C_s^TC_{sb}\widehat{M_{s1}U_2R\mathbf{e}_i}\gamma \\ &+ C_s^TC_{ss}\widehat{M_{s2}U_2R\mathbf{e}_i}\gamma - C_{nb}^TC_b^TC_b\widehat{M_{s1}U_2R\mathbf{e}_i}\lambda). \end{aligned} \tag{24}$$

Recalling that $-\lambda = \Lambda\gamma + \tau$,

$$\begin{aligned} LXM_2^{-1}K_2M_2^{-1}R\mathbf{e}_i = LXM_2^{-1}U_2^T[&(C_s^TC_{sb}\widehat{M_{s1}U_2R\mathbf{e}_i} \\ &+ C_s^TC_{ss}\widehat{M_{s2}U_2R\mathbf{e}_i} + C_{nb}^TC_b^TC_b\widehat{M_{s1}U_2R\mathbf{e}_i}\Lambda)\gamma \\ &+ C_{nb}^TC_b^TC_b\widehat{M_{s1}U_2R\mathbf{e}_i}\tau]. \end{aligned} \tag{25}$$

2.3.3. Control law

From Eqs. (17) and (25), one can simplify this into a compact matrix form $\mu = \Gamma\gamma$ with definitions of μ_i and Γ_i, in which μ is the stack of each μ_i matrix and Γ is similarly a stack of each Γ_i matrix.

$$\mu = \Gamma\gamma \tag{26}$$

$$\begin{aligned} \mu_i = &\left(L\widetilde{W}M_2^{-1}R + \Psi L\dot{X}M_2^{-1}R + \Phi LXM_2^{-1}R - \Phi\bar{Y}\right)\mathbf{e}_i \\ &- LXM_2^{-1}U_2^TC_{nb}^TC_b^TC_b\widehat{M_{s1}U_2R\mathbf{e}_i}\tau \end{aligned} \tag{27}$$

$$\begin{aligned} \Gamma_i = LXM_2^{-1}U_2^T(&C_s^TC_{sb}\widehat{M_{s1}U_2R\mathbf{e}_i} + C_s^TC_{ss}\widehat{M_{s2}U_2R\mathbf{e}_i} \\ &+ C_{nb}^TC_b^TC_b\widehat{M_{s1}U_2R\mathbf{e}_i}\Lambda). \end{aligned} \tag{28}$$

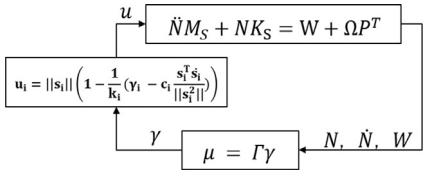

Fig. 1. Close loop system, where u is control input and u_i is the rest length of the ith string, given by Eq. (30).

Since control variable γ is composed of force densities of the strings, it also satisfies $\gamma \geq 0$ (strings are always in tension), the least square problem we choose to solve at each increment of real time Δt, is min $||\mu - \Gamma\gamma||^2,\ \gamma \geq 0$. Let the rest length of the ith string be denoted by s_{i0}, extensional stiffness by k_i, damping constant by c_i, and string vector by $\mathbf{s}_i$. Assuming that strings follow Hooke's law and the viscous friction damping model, the tension in a string is:

$$\gamma_i = \frac{||\mathbf{t}_i||}{||\mathbf{s}_i||} = \begin{cases} k_i\left(1 - \dfrac{\mathbf{s}_{i0}}{||\mathbf{s}_i||}\right) + c_i\dfrac{\mathbf{s}_i^T\dot{\mathbf{s}}_i}{||\mathbf{s}_i||^2} & \text{if } ||\mathbf{s}_i|| \geq \mathbf{s}_{i0} \\ 0 & \text{if } ||\mathbf{s}_i|| < \mathbf{s}_{i0} \end{cases}. \tag{29}$$

Then, we have rest length $\mathbf{s}_{i0}$:

$$\mathbf{s}_{i0} = ||\mathbf{s}_i||\left[1 - \frac{1}{k_i}\left(\gamma_i - c_i\frac{\mathbf{s}_i^T\dot{\mathbf{s}}_i}{||\mathbf{s}_i||^2}\right)\right]. \tag{30}$$

We can also write the string tension (a product of string length and string force density) in a matrix form:

$$T = S\hat{\gamma} = (S - S_0)\hat{k} + S\lfloor S^T\dot{S}\rfloor\lfloor S^T S\rfloor^{-1}\hat{c}, \tag{31}$$

where $S_0 = S\lfloor S^T S\rfloor^{-\frac{1}{2}}\hat{\mathbf{s}}_0$ represents the matrix containing the rest length vectors. The overall control system is shown in Fig. 1.

3. Tensegrity airfoil design

This section focuses on an error bound method for the discretization of continuous airfoils and a representation of the tensegrity airfoil topology based on matrix notations.

3.1. Error bound method

Let us assume the cord length of an airfoil is 1, the number of discrete points is p. There are two widely used spacing methods (evenly and cosine spacing) for discretizing an airfoil in the computational fluid dynamics (CFD) field [37,38]. The definition of evenly and cosine spacing is the x-coordinates of the discrete points on the airfoil satisfy a linear function $x_i = \frac{i}{p},\ (i = 1, 2, 3, \ldots, p)$ or a cosine function $x_i = 0.5[1 - \cos(\frac{\pi}{p}i)], (i = 1, 2, 3, \ldots, p)$. However, these two methods could not quantify the shape accuracy of the discretized shape compared to a continuous shape. In other words, one cannot specify how big the shape error is merely by the control points one uses. It might not bother much when one is allowed to have a sufficient number of discrete points, but when it comes to describing an airfoil with limited points, it reveals the importance to obtain a better discrete shape. In consequence, this paper proposes an error bound spacing method, see Fig. 2, which discretizes an airfoil and provides a quantitative representation of airfoil shape accuracy. This may improve the performance prediction of airfoil designs.

Error bound method: Given the exact airfoil shape, approximate the shape with straight-line segments. Choose the location of the nodes of the straight-line segments such that the maximum error between the defined shape and each straight-line segment is less than a specified value δ.

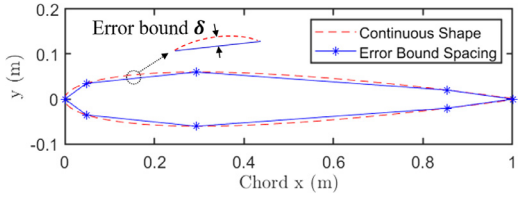

Fig. 2. Illustration of error bound spacing method by NACA0012 with error bound $\delta = 0.008$ m.

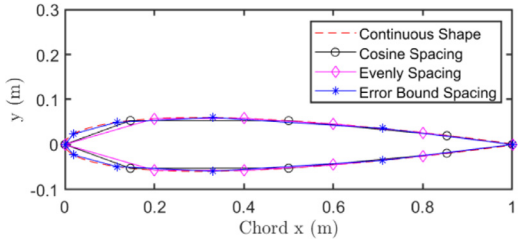

Fig. 3. Comparison of cosine spacing, evenly spacing, and error bound spacing methods by NACA0012 with same amount of discrete points.

Following the definition, an algorithm can be formulated to obtain the coordinates of the discrete points, shown in Algorithm 1. Let an example to illustrate the advantage of the error bound method comparing with evenly and cosine spacing ones, shown in Fig. 3. It is clear that the error bound method has better accuracy for the same number of discrete points, and the error bound δ also provides a quantitative sense of the accuracy of the discrete airfoil.

Algorithm 1: Error Bound Spacing Algorithm

1) Let $y = f(x),\ x \in [0, 1]$ be the function of a continuous airfoil shape, an error bound value be δ.
2) Let $x_0 \in x$ be the start point of discretization, then $x \in [0, x_0]$ is the continuous part (called the "D-Section") and $x \in [x_0, 1]$ is the discrete part.
3) Let (x_2, y_2) be the next discrete point, the line function of segment (x_0, y_0) and (x_2, y_2) is:
$Ax + By + C = 0,$ (32)
where $A = y_2 - y_0,\ B = -1,$ and $C = y_0 - Ax_0$.
4) The point $(x_1, y_1), x_1 \in (x_0, x_2)$ has the largest distance with the line segment:
$d = \frac{|Ax_1 + By_1 + C|}{\sqrt{A^2 + B^2}}$. (33)
5) Obtain all the discrete points:
while $x \leq 1$ **do**
  $f'(x)|_{x=x_1} = \frac{y_2 - y_0}{x_2 - x_0}$
  $\frac{||Ax_1 + By_1 + C||}{\sqrt{A^2 + B^2}} = \delta$, solve for x_2
  Store (x_2, y_2) and update $x_0 \leftarrow x_2$.
end while

3.2. Topology of tensegrity airfoil

Having located the nodes of the straight-line approximation of the desired shape, we now must show the interior tensegrity structure of the airfoil. Inspired by vertebrae, we connect the discrete points in a similar pattern shown in Fig. 4, where the black and lines represent rigid members (bars) and tendons (strings). The D-section, also called D-box, is a structure in a letter D form in the front of the airfoil widely used in wing structure construction. This topology design is intuitive, compact, but effective for

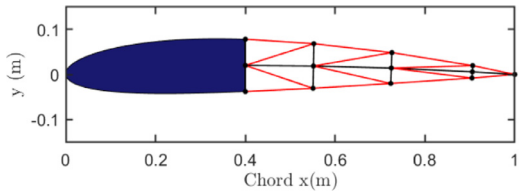

Fig. 4. Tensegrity topology of airfoil NACA2412 with shape error bound $\delta = 0.001$ m, along the chord 0–0.4 m (the shaded blue area) is 'Rigid Structure', and 0.4–1 m (the black and red lines) is 'Flexible Structure'. (For interpretation of the references to color in this figure legend, the reader is referred to the web version of this article.)

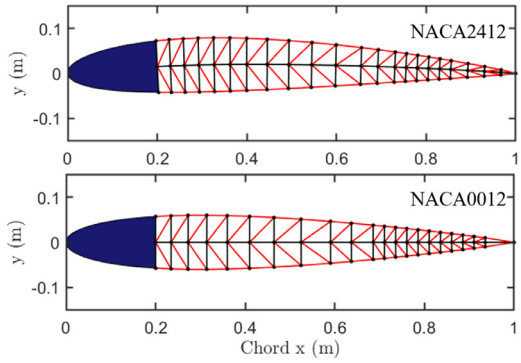

Fig. 5. Tensegrity airfoil topology, error bound $\delta = 1.0 \times 10^{-4}$ m, along the chord 0–0.2 m (the shaded blue area is the D-Section), NACA0012 (structure complexity $q = 21$) and NACA2412 (structure complexity $q = 22$). (For interpretation of the references to color in this figure legend, the reader is referred to the web version of this article.)

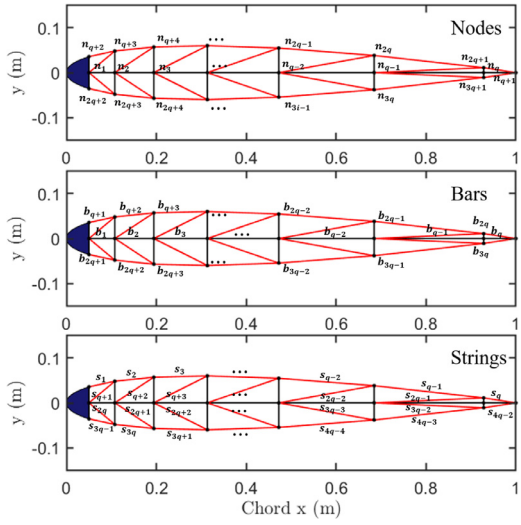

Fig. 6. Node, bar, and string notations of a tensegrity airfoil with complexity q. (For interpretation of the references to color in this figure legend, the reader is referred to the web version of this article.)

shape control ability. We define a tensegrity airfoil of complexity q as the number of groups of vertical bars. Examples of an asymmetric and asymmetric airfoil with high complexity are shown in Fig. 5.

3.3. General modeling of tensegrity airfoil

To generate a tensegrity airfoil with any complexity q, the first thing is to define nodal, bar connectivity, and string connectivity matrices: N, C_b, and C_s. The nodal matrix N contains the vectors of all the nodes and labeling bars and strings as shown in Fig. 6,

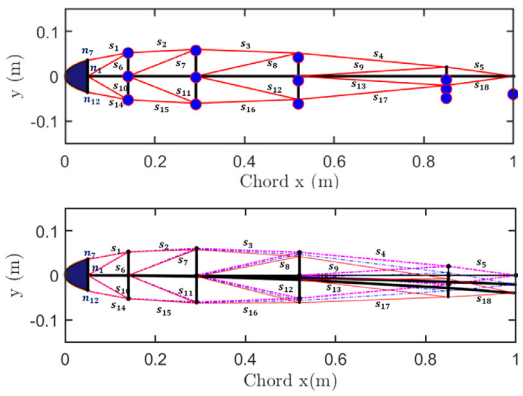

Fig. 7. Tensegrity NACA0012, error bound $\delta = 0.002$ m, along the chord 0–0.05 m, control objectives are big blue dots in the upper plot. There are three-time history plots in the lower figure, the magenta dotted lines are at 0 s, the blue lines are at 7 s, and the red lines are at the 20 s. (For interpretation of the references to color in this figure legend, the reader is referred to the web version of this article.)

one can write C_b and C_s by starting with each unit coordinates. $C_{b_{in}}$ and $C_{s_{in}}$ whose two elements in each row denotes the start and end node of one bar or string:

$$C_{b_{in}} = \begin{cases} [i, i+1], & 1 \le i \le q \\ [i-q, i+1], & q+1 \le i \le 2q \\ [i-2q, i+1], & 2q+1 \le i \le 3q \end{cases}, \tag{34}$$

$$C_{s_{in}} = \begin{cases} [i+1+q, i+2+q], & 1 \le i \le q-1 \\ [2q+1, q+1] \\ [i-q, i+2], & q+1 \le i \le 2q-1 \\ [i-2q+1, i+3], & 2q \le i \le 3q-2 \\ [i+3-q, i+4-q], & 3q-1 \le i \le 4q-3 \\ [3q+1, q+1] \end{cases}. \tag{35}$$

Then a function can be written to convert $C_{b_{in}}$ and $C_{s_{in}}$ to C_b and C_s [39].

4. Numerical study of a morphing airfoil

The primary goal of describing the kinematics of a flexible foil (i.e. fish swimming and wing flapping) is helping researchers study the fundamental motion mechanism and recreate the similar efficient flow types. In this study, we implement NACA0012 (D-Section 0–0.05 m, error bound $\delta = 0.002$ m) to evaluate the performance of the controller. The control objective is to transform the airfoil from one shape to another, shown in the upper part of Fig. 7. The morphing targets described in [40], which are:

$$y(x,t) = \begin{cases} 0, & 0 \le x \le c_{rgd} \\ A_0 \left(\frac{x - c_{rgd}}{c - c_{rgd}}\right)^2 sin\left(\frac{\pi}{2} t\right), & c_{rgd} \le x \le c \end{cases}, \tag{36}$$

where A_0 is the maximum amplitude achieved at the trailing edge of the airfoil, c is the cord length, the rigid part is c_{rgd} ($c_{flex} = c - c_{rgd}$), A is the amplitude envelop, x is coordinate along the cord, and $t = [0, 1]$ s (tail bends maximum at one fourth of a period). Then, based on Eq. (36), coordinates of control targets $\bar{Y}$ can be calculated. In the control simulation, amplitude $A_0 = -0.04$ m, time step $dt = 0.001$ s, stability coefficients $\Psi = 2.5$ and $\Phi = 4$, mass of the longest bar and string are 1 kg and 0.01 kg, and the masses of the shorter bars and strings are scaled accordingly. Nodes n_1, n_{q+2}, and n_{2q+2} in Fig. 6 are fixed with the D-Section, in our case structure complexity $q = 5$, n_1, n_7, and n_{12} are not controlled. Since we

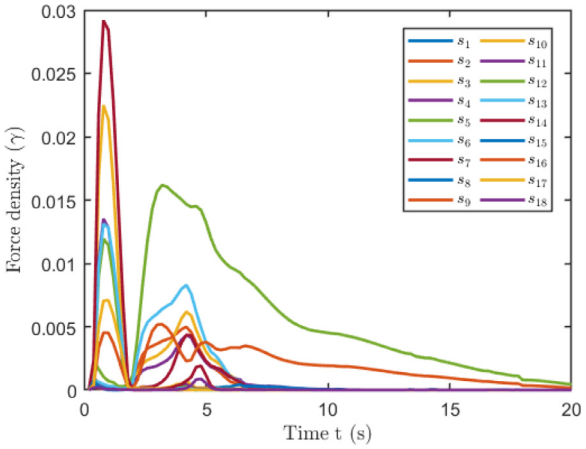

Fig. 8. Force densities of all the strings, string labels can be found in Fig. 7.

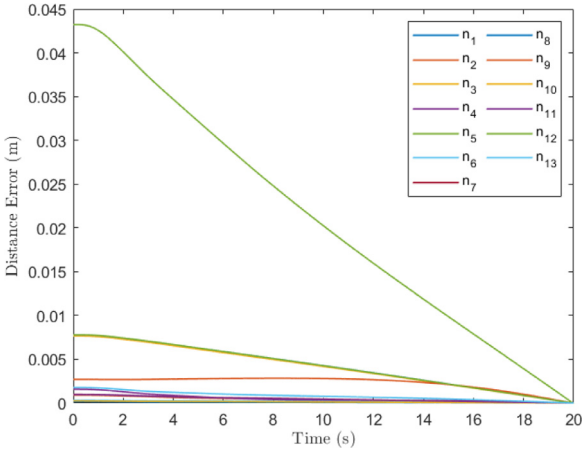

Fig. 9. Distance error between current node position and the target position with respect to time, node labels can be found in Fig. 7.

are controlling x and y coordinates, matrix $L = [1\ 0\ 0; 0\ 1\ 0; 0\ 0\ 0]$, matrix $R^{16\times 13}$ (generated by $I^{16\times 16}$ with columns 1, 7 and 12 being deleted).

The time-lapse in Fig. 7 shows that the desired shape transformation is achieved in 20 s. For the above simulation, string tensions drive the desired shape transformation. To illustrate this, force densities (γ) time history is shown in Fig. 8. Fig. 9 shows the distance error between the current node positions to the target respect to time, which demonstrates the successful shape control at a final time.

5. Conclusion

This paper offers an approach to integrate structure and control design. Based on the non-linear reduced-order class-k tensegrity dynamics, a non-linear control law is derived. The control variables (force densities in strings) appear linearly in the non-linear dynamics. An airfoil discretization method to bound the local error of each node is introduced and combined with the design of tensegrity airfoils. An example is given to demonstrate the feasibility of shape control of tensegrity airfoils. The approach can also be used for design and shape control of other tensegrity structures.

Declaration of Competing Interest

The authors whose names are listed immediately below certify that they have NO affiliations with or involvement in any organization or entity with any financial interest (such as honoraria; educational grants; participation in speakers bureaus; membership, employment, consultancies, stock ownership, or other equity interest; and expert testimony or patent-licensing arrangements), or non-financial interest (such as personal or professional relationships, affiliations, knowledge or beliefs) in the subject matter or materials discussed in this manuscript.

CRediT authorship contribution statement

Muhao Chen: Conceptualization, Methodology, Software.

Acknowledgments

The authors thank Mr. Xiaolong Bai for his many helpful discussions.

References

[1] G. Padfield, B. Lawrence, The birth of flight control: an engineering analysis of the Wright brothers' 1902 glider, Aeronaut. J. 107 (1078) (2003) 697–718.
[2] A. Sofla, S. Meguid, K. Tan, W. Yeo, Shape morphing of aircraft wing: status and challenges, Mater. Des. 31 (3) (2010) 1284–1292.
[3] X. Lachenal, S. Daynes, P.M. Weaver, Review of morphing concepts and materials for wind turbine blade applications, Wind Energy 16 (2) (2013) 283–307.
[4] K. Kuribayashi, K. Tsuchiya, Z. You, D. Tomus, M. Umemoto, T. Ito, M. Sasaki, Self-deployable origami stent grafts as a biomedical application of Ni-rich tini shape memory alloy foil, Mater. Sci. Eng. A 419 (1–2) (2006) 131–137.
[5] K. Liu, J. Wu, G.H. Paulino, H.J. Qi, Programmable deployment of tensegrity structures by stimulus-responsive polymers, Sci. Rep. 7 (1) (2017) 3511.
[6] J. Valasek, Morphing Aerospace Vehicles and Structures, 57, John Wiley & Sons, 2012.
[7] S. Barbarino, O. Bilgen, R.M. Ajaj, M.I. Friswell, D.J. Inman, A review of morphing aircraft, J. Intell. Mater. Syst. Struct. 22 (9) (2011) 823–877.
[8] G. Reich, B. Sanders, Introduction to morphing aircraft research, J. Aircraft 44 (4) (2007). 1059–1059
[9] M. Santer, S. Pellegrino, Topology optimization of adaptive compliant aircraft wing leading edge, in: Proceedings of the 48th AIAA/ASME/ASCE/AHS/ASC Structures, Structural Dynamics, and Materials Conference, 2007, p. 1714.
[10] M. Santer, S. Pellegrino, Topological optimization of compliant adaptive wing structure, AIAA J. 47 (3) (2009) 523–534.
[11] R.E. Skelton, M.C. de Oliveira, Tensegrity Systems, 1, Springer, 2009.
[12] R.E. Skelton, K. Nagase, Tensile tensegrity structures, Int. J. Space Struct. 27 (2–3) (2012) 131–137.
[13] P. Foti, A. Fraddosio, S. Marzano, G. Pavone, M.D. Piccioni, On self-equilibrium state of v-expander tensegrity beam-like grids, Res. Eng. Struct. Mater. 4 (1) (2018) 16.
[14] A. Fraddosio, G. Pavone, M.D. Piccioni, Minimal mass and self-stress analysis for innovative v-expander tensegrity cells, Compos. Struct. 209 (2019) 754–774.
[15] J.J. Rimoli, R.K. Pal, Mechanical response of 3-dimensional tensegrity lattices, Compos. Part B: Eng. 115 (2017) 30–42.
[16] J. Chen, W. Friesen, T. Iwasaki, Mechanisms underlying rhythmic locomotion: body–fluid interaction in undulatory swimming, J. Exp. Biol. 214 (4) (2011) 561–574.
[17] L.-H. Chen, K. Kim, E. Tang, K. Li, R. House, E.L. Zhu, K. Fountain, A.M. Agogino, A. Agogino, V. Sunspiral, E. Jung, Soft spherical tensegrity robot design using rod-centered actuation and control, J. Mech. Robot. 9 (2) (2017) 025001.
[18] C. Paul, F.J. Valero-Cuevas, H. Lipson, Design and control of tensegrity robots for locomotion, IEEE Trans. Robot. 22 (5) (2006) 944–957.
[19] R. Skelton, F. Fraternali, G. Carpentieri, A. Micheletti, Minimum mass design of tensegrity bridges with parametric architecture and multiscale complexity, Mech. Res. Commun. 58 (2014) 124–132.
[20] G. Tibert, Deployable Tensegrity Structures for Space Applications, KTH, 2002 Ph.D. thesis.
[21] K. Pajunen, P. Johanns, R.K. Pal, J.J. Rimoli, C. Daraio, Design and impact response of 3D-printable tensegrity-inspired structures, Mater. Des. 182 (2019) 107966.
[22] E.A. Peraza Hernandez, R. Goyal, R.E. Skelton, Tensegrity structures for mass–efficient planetary landers, in: Proceedings of the IASS Annual Symposia, 2018, International Association for Shell and Spatial Structures (IASS), 2018, pp. 1–8.
[23] J.J. Rimoli, On the impact tolerance of tensegrity-based planetary landers, in: Proceedings of the 57th AIAA/ASCE/AHS/ASC Structures, Structural Dynamics, and Materials Conference, 2016, p. 1511.
[24] V. SunSpiral, G. Gorospe, J. Bruce, A. Iscen, G. Korbel, S. Milam, A. Agogino, D. Atkinson, Tensegrity based probes for planetary exploration: entry, descent and landing (EDL) and surface mobility analysis, Int. J. Planet. Probes 7 (2013) 13.
[25] L. Zhao, E.A.P. Hernandez, Theoretical study of tensegrity systems with tunable energy dissipation, Extreme Mech. Lett. 32 (2019) 100567.
[26] A.P. Sabelhaus, A.K. Akella, Z.A. Ahmad, V. SunSpiral, Model-predictive control of a flexible spine robot, in: Proceedings of the 2017 American Control Conference (ACC), IEEE, 2017, pp. 5051–5057.

[27] A.P. Sabelhaus, H. Ji, P. Hylton, Y. Madaan, C. Yang, A.M. Agogino, J. Friesen, V. SunSpiral, Mechanism design and simulation of the ultra spine: a tensegrity robot, in: Proceedings of the ASME 2015 International Design Engineering Technical Conferences and Computers and Information in Engineering Conference, American Society of Mechanical Engineers Digital Collection, 2015.
[28] J.V. Henrickson, R.E. Skelton, J. Valasek, Shape control of tensegrity airfoils, in: Proceedings of the AIAA Guidance, Navigation, and Control Conference, 2016, p. 1864.
[29] K.W. Moored, H. Bart-Smith, The analysis of tensegrity structures for the design of a morphing wing, J. Appl. Mech. 74 (4) (2007) 668–676.
[30] K.W. Moored, S.A. Taylor, T.K. Bliss, H. Bart-Smith, Optimization of a tensegrity wing for biomimetic applications, in: Proceedings of the 45th IEEE Conference on Decision and Control, IEEE, 2006, pp. 2288–2293.
[31] M. Jones, K. Cohen, Fuzzy control of a tensegrity based morphing UAV wing, in: Proceedings of the Infotech@ Aerospace 2011, 2011, p. 1561.
[32] A. Jameson, Aerodynamic design via control theory, J. Sci. Comput. 3 (3) (1988) 233–260.
[33] R. Motro, S. Najari, P. Jouanna, Static and dynamic analysis of tensegrity systems, in: Shell and Spatial Structures: Computational Aspects, Springer, 1987, pp. 270–279.
[34] R.E. Skelton, J.P. Pinaud, D.L. Mingori, Dynamics of the shell class of tensegrity structures, J. Frankl. Inst. 338 (2-3) (2001) 255–320.
[35] R. Goyal, R.E. Skelton, Tensegrity system dynamics with rigid bars and massive strings, Multib. Syst. Dyn. 46 (2019) 203–228, doi:10.1007/s11044-019-09666-4.
[36] J. Cheong, R.E. Skelton, Nonminimal dynamics of general class k tensegrity systems, Int. J. Struct. Stab. Dyn. 15 (02) (2015) 1450042.
[37] C.L. Ladson, C.W. Brooks Jr., A.S. Hill, D.W. Sproles, Computer Program to Obtain Ordinates for NACA Airfoils (1996).
[38] L. Leifsson, S. Koziel, Aerodynamic shape optimization by variable-fidelity computational fluid dynamics models: a review of recent progress, J. Comput. Sci. 10 (2015) 45–54.
[39] R. Goyal, M. Chen, M. Majji, R. Skelton, Motes: modeling of tensegrity structures, J. Open Sour. Softw. 4 (42) (2019) 1613, doi:10.21105/joss.01613.
[40] N. Li, H. Liu, Y. Su, Numerical study on the hydrodynamics of thunniform bio-inspired swimming under self-propulsion, PloS One 12 (3) (2017) e0174740.